



**Acoustics'08
Paris**
June 29-July 4, 2008
www.acoustics08-paris.org

LDV measurements of acoustic streaming in a traveling wave, closed-loop resonator

Cyril Desjoux, Pierrick Lotton, Guillaume Penelet and James Blondeau

Laboratoire d'Acoustique de l'Université du Maine, Avenue Olivier Messiaen, 72085 Le Mans,
France

cyril.desjoux@univ-lemans.fr

This work deals with the study of an annular acoustic resonator, where the acoustic field is controlled by two loudspeakers in order to generate a purely traveling wave. In the first part of this paper, the theoretical acoustic field in this device is described by an electroacoustic modeling and compared to the experimental results. The second part deals with the characterization of non-linear effects occurring in such a device. The generation of acoustic streaming is especially investigated in our study. Laser Doppler Velocimetry measurements are performed in order to characterize both first order (acoustic) and second order (acoustic streaming) velocity fields. Works are now in progress in order to improve the accuracy of streaming measurements and to compare the experimental data to the available theories. This study should contribute to enhance the designing of thermoacoustic devices and should have practical applications in microfluidics, especially in frame of micro-pumps and micro-mixers development.

1 Introduction

Many thermoacoustic engines have been developed and studied for the last twenty years. However the classical linear theory of thermoacoustic [1, 2] is inadequate to describe the complexity of some non linear effects occurring in such devices, such as the generation of acoustic streaming, i.e an acoustically induced mean fluid flow, which disturbs the temperature field with subsequent variations of the acoustic field. Many researches have been driven last years to describe this acoustic streaming in standing wave thermoacoustic resonators [3, 4, 5], but a few yet in traveling wave thermoacoustic resonators [6, 7, 8, 9], where the existence of a loop allows the average flow to be non zero through a cross section of the resonator. The aim of this paper is to propose an experimental characterization of such a streaming in an annular resonator.

The device studied in this paper is not a thermoacoustic engine. This is an annular waveguide, where the acoustic field is controlled by two loudspeakers appropriately placed and phased in order to generate a traveling wave (Fig. 1). Each driver generates two counter-propagating harmonic plane waves. The complex amplitude $\tilde{p}(x)$ of the acoustic pressure field $p(x, t) = \text{Re} [\tilde{p}(x) e^{j\omega t}]$ is the sum of four traveling plane waves written

$$\tilde{p}(x) = \tilde{p}^+(x_1) e^{-jk(x-x_1)} + \tilde{p}^-(x_1) e^{-jk(x+x_1)} \quad (1)$$

$$+ \tilde{p}^+(x_2) e^{-jk(x-x_2)} e^{j\phi} + \tilde{p}^-(x_2) e^{-jk(x+x_2)} e^{j\phi},$$

where $k = 2\pi/\lambda$ is the acoustic wave number and ϕ is the phase shift between the sources. Then, if each driver has the same amplitude displacement (so leading the acoustic pressures to $\tilde{p}^\pm(x_1) = \tilde{p}^\pm(x_2) = \tilde{P}_0$), if the wave-length λ is equal to the unwrapped length of the resonator $L = 2\pi R_0$ and if the phase and the distance between the two sources are respectively $\pi/2$ and $L/4$, acoustic pressure field is $\tilde{p}(x) = 2\tilde{P}_0 e^{-jk(x-x_1)}$, which is the formulation for a purely traveling wave.

Only a few works dealing with such kind of device have been carried out [10, 11]. There already exists some kind of ultrasonic motors [12] or some looped-tube thermoacoustic engines [13], but to the best of our knowledge, no experimental works have been published on our particular device. So this is why the present study has been led, for its interest in thermoacoustics, but also in microfluidics, for the development of size reduced systems like micro-pumps and micro-mixers [14].

Section 2 of this paper contains a description of the experimental device. Section 3 provides theoretical elements to calculate acoustic field in an annular wave-

guide and some experimental Laser Doppler Velocimetry (LDV) results concerning acoustic field. Section 4 gives results of LDV streaming velocity measurement.

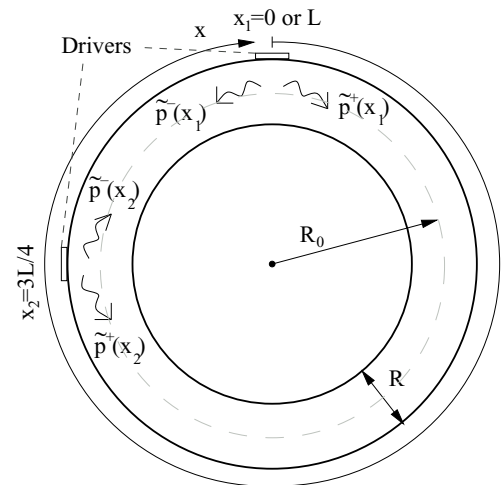


Figure 1: Diagram of the closed-loop resonator.

2 Experimental device

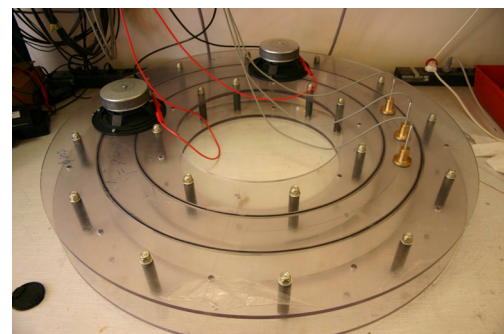


Figure 2: Experimental device photograph.

Fig. 1 and Fig. 2 show the experimental annular resonator. Its square cross section is 7.5×7.5 cm and its unwrapped length L is about 2.12 m. Two electrodynamic transducers (Audax PR170MO), located at positions $x = 0$ and $x = 3L/4$, sustain an acoustic wave at a frequency corresponding to the first natural mode of the air column ($f = 161$ Hz). Phase and amplitude of the drivers displacements are controlled in order to produce standing or traveling waves. Three electrostatic microphones (Brüel&Kjaer 4136 at $x = 0.41$ m, $x = 0.55$ m and $x = 0.67$ m) monitor amplitude and phase of

acoustic pressure in these three points, allowing to describe the acoustic field in all the domain $x \in [0, L]$ [15]. The waveguide, filled with air, is made of plexiglass to allow LDV measurements of acoustic and streaming velocities. Small cork closed holes allow to introduce the smoke from burned wooden sawdust before LDV measurements. Smoke particles are cool down through cold water before their introduction in the waveguide. LDV and microphone measurements are realized at atmospheric pressure and at a temperature of 20° C. The LDV system (Dantec FlowLite) allows to measure axial component of acoustic and streaming velocity. The laser (HeNe) has an optical wavelength of 532 nm and a power of 10 mW. Measurement volume is about 0.05 mm (direction measurement) \times 0.43 mm (width) \times 0.05 with a probe equipped with a 160 mm standard front lens. The LDV probe is mounted on a system moving in the transverse direction with a displacement precision of 1 μ m. The waveguide itself is mounted on a rotating board which allows to make measurements along the axial direction. The signal is captured by a photomultiplier and analysed by the BSA system (Burst Spectrum Analyzer). Computer acquisitions allow a post-treatment of results. Rotating machine algorithm brings back all samples on a single acoustic period ; the average value (over an acoustic period) of the signal then corresponds to the streaming velocity, while the oscillating component corresponds to acoustic velocity.

3 Acoustic field

Complex amplitudes of the acoustic pressure $\tilde{p}(x, t)$ and the acoustic volumetric flow $\tilde{u}(x, t)$ are written, in region I ($x \in [0, 3L/4]$),

$$\tilde{p}_I(x) = \tilde{p}_0^+ e^{-ik_0 x} + \tilde{p}_0^- e^{+ik_0 x}, \quad (2)$$

$$\tilde{u}_I(x) = \frac{S_w}{\rho_0 c_0} [\tilde{p}_0^+ e^{-ik_0 x} - \tilde{p}_0^- e^{+ik_0 x}], \quad (3)$$

and in region II ($x \in [3L/4, L]$),

$$\tilde{p}_{II}(x) = \tilde{p}_L^+ e^{-ik_0(x-L)} + \tilde{p}_L^- e^{+ik_0(x-L)}, \quad (4)$$

$$\tilde{u}_{II}(x) = \frac{S_w}{\rho_0 c_0} [\tilde{p}_L^+ e^{-ik_0(x-L)} - \tilde{p}_L^- e^{+ik_0(x-L)}], \quad (5)$$

where $k_0 = \omega/c_0$ is the wave number with $\omega = 2\pi f$, and where \tilde{p}_0^\pm and \tilde{p}_L^\pm are complex amplitudes of acoustic pressure at $x = 0$ and $x = L$. Pressure and flow continuity equations take, for $x = 0$, the forms

$$\tilde{p}_0^+ + \tilde{p}_0^- = \tilde{p}_L^+ + \tilde{p}_L^- = \tilde{p}_1, \quad (6)$$

$$\frac{S_w}{\rho_0 c_0} (\tilde{p}_0^+ - \tilde{p}_0^-) = \frac{S_w}{\rho_0 c_0} (\tilde{p}_L^+ - \tilde{p}_L^-) + \tilde{U}_1, \quad (7)$$

and, for $x = 3L/4$, the forms,

$$\begin{aligned} \tilde{p}_0^+ e^{-ik_0 3L/4} + \tilde{p}_0^- e^{+ik_0 3L/4} \\ = \tilde{p}_L^+ e^{+ik_0 L/4} + \tilde{p}_L^- e^{-ik_0 L/4} = \tilde{p}_2, \end{aligned} \quad (8)$$

$$\frac{S_w}{\rho_0 c_0} (\tilde{p}_0^+ e^{-ik_0 3L/4} - \tilde{p}_0^- e^{+ik_0 3L/4}) \quad (9)$$

$$= \frac{S_w}{\rho_0 c_0} (\tilde{p}_L^+ e^{+ik_0 L/4} - \tilde{p}_L^- e^{-ik_0 L/4}) - \tilde{U}_2,$$

where $\tilde{p}_{1,2}$ and $\tilde{U}_{1,2}$ correspond to the acoustic pressures

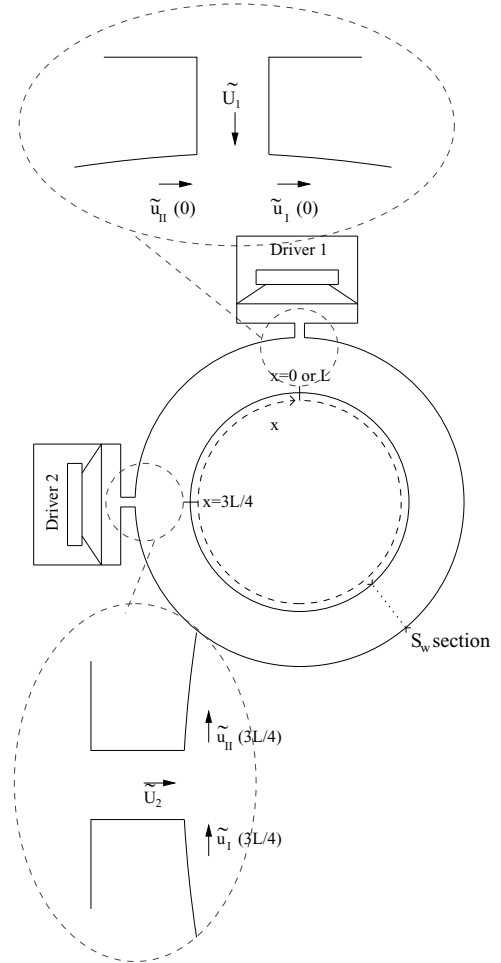


Figure 3: Diagram of experimental device.

and acoustic volumetric flows at positions $x = 0$ and $x = 3L/4$, respectively (in the two tubes coupling the sources and the waveguide).

The driver i ($i = 1$ or 2) and its load are represented by the electroacoustic equivalent network given on Fig. 4 when the driver j ($j = 2$ or 1) is turned off. On this network, Z_{ls_i} represents the acoustic impedance equivalent to the electromechanical part of the loudspeaker, C_{ar} represents the acoustic compliance of the rear cavity, C_{av} the acoustic compliance of the front cavity, M_a the acoustic mass localized in the tube coupling the front cavity and the resonator, R_a the resistance localized in this tube, and $Z_{ter_i} = \tilde{p}_i/\tilde{U}_i$ represent the input impedance of the resonator. This input impedance takes into account the presence of the turned off driver j of which the impedance is denoted Z_{s_j} (Fig. 5).

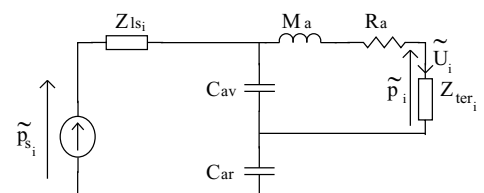


Figure 4: Electrical equivalent circuit of source i (at $x = 0$ for $i = 1$ and at $x = 3L/4$ for $i = 2$).

The use of the equivalent networks of Fig. 4 and Fig. 5, when the driver 1 ($x = 0$) is turned on and the driver 2 ($x = 3L/4$) is turned off, leads to the following

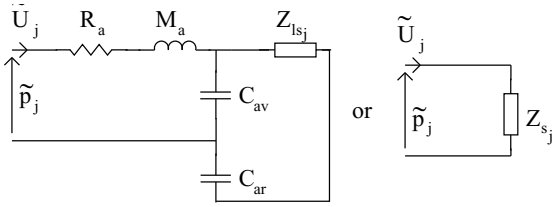


Figure 5: Electrical equivalent circuit of the acoustic impedance presented to the resonator by turned off source j (at $x = 0$ for $i = 1$ and at $x = 3L/4$ for $i = 2$).

expressions,

$$\frac{\tilde{p}_1}{\tilde{p}_{s1}} = \frac{Z_{ter1}}{Z_{ter1} + jM_a\omega + R_a} \cdot \frac{Z_{av}}{Z_{eq} + Z_{ls1}}, \quad (10)$$

$$Z_{s2} = \frac{\tilde{p}_2}{\tilde{U}_2} = R_a + jM_a\omega + \frac{\frac{1}{jC_{ar}\omega} + Z_{ls1}}{1 + \frac{C_{av}}{C_{ar}} + j\omega Z_{ls1}C_{av}}, \quad (11)$$

where Z_{av} is the first source's acoustic front load impedance, function of C_{av} , M_a , R_a and Z_{ter1} , and where Z_{eq} is the global acoustic load (front and rear).

Equations (6-11) form an eight equation system with nine unknowns, $\tilde{p}^\pm(0)$, $\tilde{p}^\pm(L)$, $\tilde{p}_{1,2}$, $\tilde{u}_{1,2}$ and \tilde{p}_{s1} . Pressure response at axial coordinate $x = 0$, $\tilde{p}_1/\tilde{p}_{s1}$, can now be found. Equations (2-5) allow next to build spacial distribution of acoustic field in all the resonator, so that pressure response $\tilde{p}(x)/\tilde{p}_{s1}$ for any axial coordinate along the resonator is finally obtained.

Then, the same approach allows to express the pressure response $\tilde{p}(x)/\tilde{p}_{s2}$ (with $\tilde{p}_{s2} = \tilde{p}_{s1}e^{j\phi}$) when the driver 2 is turned on and the driver 1 is turned off. The superposition principle drives us finally to the global transfer function. Fig. 6 shows theoretical and experimental pressure responses at coordinate $x = 0.4$ m.

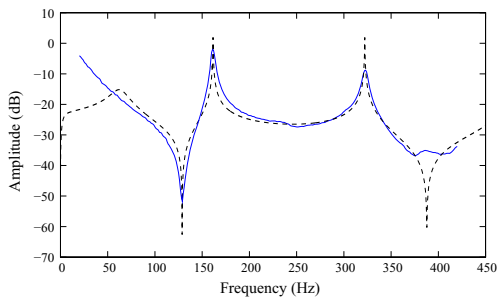


Figure 6: Experimental (continuous line) and theoretical (dashed line) transfer function $p(x)/p_{s1}$ at axial position $x = 0.4$ m when the driver 1 receives 1 V and the driver 2 is turned off.

The acoustic velocity distribution along the axial coordinate is given by Fig. 7 and Fig. 8 for a phase difference between the two loudspeakers of 0 and $\pi/2$, respectively, and the same amplitude displacement for the two drivers. These theoretical results are here compared with the LDV measurements which are all performed at the center of the cross section. When the amplitude displacement of the two drivers are phased (Fig. 7), the wave in the resonator is a standing wave. Field disturbances appear near the position of loudspeakers (i.e. at $x = 0$ or L and at $x = 3L/4$). These perturbations are produced by the connection between the waveguide

and the loudspeaker's front cavity. This connection is a 20 mm in diameter hole which may create small vortex and disturb velocity fields. A way to decrease those effects is to increase hole diameter, but this may increase coupling effects between the waveguide and the sources. When the phase difference between the two loudspeakers is $\pi/2$ (Fig. 8), the wave inside the waveguide is a traveling wave. It still exists some variations which mean that the acoustic field still have a stationary component. However the standing wave ratio is lower than 10%. The traveling wave ratio can be optimized by controlling more precisely the relative amplitude and phase of the loudspeakers.

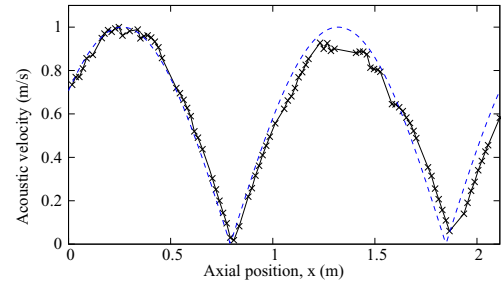


Figure 7: Normalized profiles v_{ac}/v_{max} (where v_{ac} and v_{max} are the amplitude of acoustic velocity and the maximum of acoustic velocity along the waveguide, respectively) of experimental (continuous line) and theoretical (dashed line) acoustic velocity field with respect to the axial position x for $\phi = 0$.

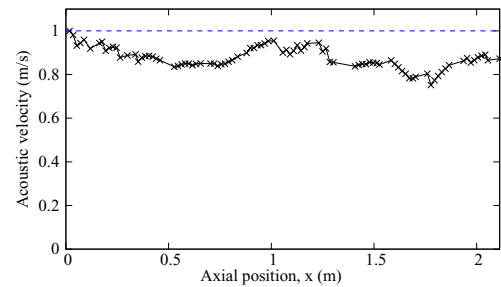


Figure 8: Normalized profiles v_{ac}/v_{max} of experimental (continuous line) and theoretical (dashed line) acoustic field with respect to the axial position x for $\phi = \pi/2$.

Fig.9 shows acoustic velocity field with respect to the transverse position. The phase shift between the two drivers is $\pi/2$ and their amplitude displacements are equals. LDV measurements are performed far away from the sources. Velocity is not constant across a section of the waveguide. This effect is due to the resonator's curvature.

4 Streaming velocity field measurement

Measurement of streaming velocity is very tricky. Many parameters, like number of smoke particles getting through the measurement volume, temperature and static pressure variations, smoke influence on density of fluid, are questioned. It appears that one of the most

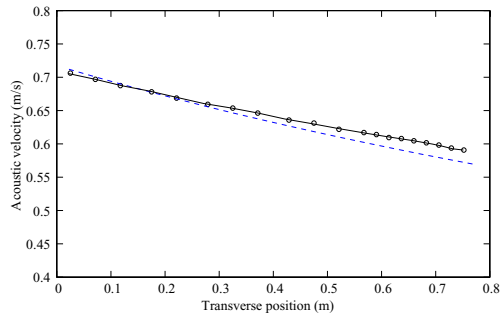


Figure 9: Profile of experimental (continuous line) and theoretical (given in dashed line by the classical linear theory of acoustic) acoustic field with respect to the transverse position.

influent effect is the stabilization time of streaming velocity field. Fig.10 and Fig.11 show variations of acoustic and streaming velocity fields after the introduction of seeding particles. While the amplitude of acoustic velocity converge to a constant value after only 20 s, streaming velocity amplitude converges to a constant value after 2000 s. It means that between each introduction of smoke particles into the waveguide, LDV measurements cannot begin before this stabilization time. However, measurements cannot be performed more than 4000 s after the introduction of seeding particles, due to the graduate decrease of seeding particles quantity with subsequent decrease of signal to noise ratio.

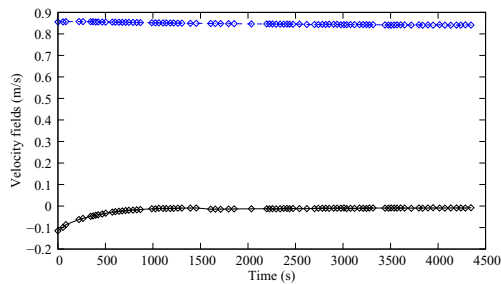


Figure 10: Variations of measured acoustic (dashed line) and streaming (continuous line) velocities with respect to time, after introducing seeding particles.

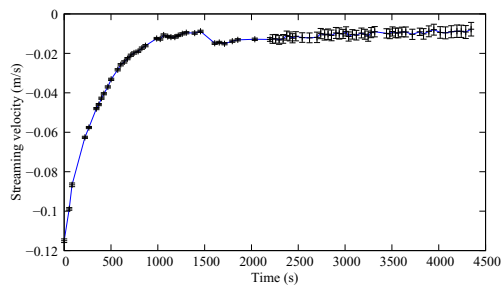


Figure 11: Variations of measured streaming velocity with respect to time, after introducing seeding particles (zoom of Fig. 10).

Streaming velocity through a section of the waveguide is not symmetrical with respect to the center axis (Fig.12). This is due to the acoustic velocity which is not constant on the resonator section. This acoustic velocity variation acts inevitably on the streaming velocity

distribution. From the transverse coordinate 0 to the coordinate R (from inner to outer radius of the annular resonator) the uncertainties decrease, because there are less smoke particles near the inner radius than near the outer radius.

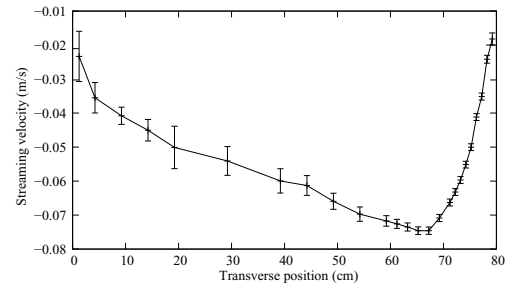


Figure 12: Profile of streaming velocity field with respect to the transverse position.

The quadratic dependence of the streaming velocity with respect to the acoustic pressure [16], $v_s = \alpha p_{ac}^2$ (where v_s is the streaming velocity, p_{ac} is the acoustic pressure and α a proportionality factor) is checked at a fix point (Fig.13), far away from drivers and at the center of the waveguide section. The value of alpha is adjusted (here, $\alpha = 0.3 \cdot 10^{-7}$) to fit experimental results.

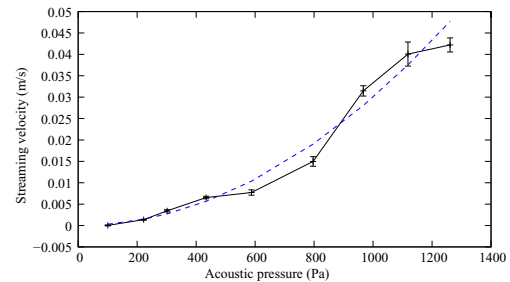


Figure 13: Experimental (continuous line) and theoretical (dashed line) streaming velocity with respect to the acoustic pressure amplitude.

5 Conclusion

In this paper, the analytical and experimental study of a traveling wave closed-loop resonator has been presented. An electroacoustic model is presented which describes the coupling between the two drivers and the resonator. The distribution of the acoustic field, which is controlled both by the relative driving amplitude and phase shift between the two loudspeakers, is also measured using LDV and compared with the model. The experimental analysis of the acoustic streaming development is also carried out using LDV. It is shown that this measurement is quite difficult to manage, due to its strong sensitivity to environment parameters and to the quality of seeding (stabilization time, number of smoke particles...). However, our preliminary results allow us to check the quadratic dependence with acoustic pressure of the acoustic streaming velocity, and the analysis of the transverse profile of acoustic streaming distribution shows an asymmetric profile which is attributed to the waveguide's curvature. Works are now in progress in

order to characterize more deeply the development of acoustic streaming in such a device, and to compare the experimental results to an adequate numerical model. The effect of the introduction of a stack in the waveguide will be also investigated in the future.

6 Acknowledgments

This work was supported by the french National Research Agency (contract number ANR-05-BLANC-0016-2).

References

- [1] Rott N., "Thermoacoustics", *Adv. Appl. Mech.*, **20** 135-175 (1980)
- [2] Swift G.W., "Thermoacoustic engines", *J. Acoust. Soc. Am.*, **84** (4) 1145-1179 (1988)
- [3] Thompson M.W., Atchley A.A., "Simultaneous measurement of acoustic and streaming velocities in a standing wave using laser Doppler anemometry", *J. Acoust. Soc. Am.*, **117** (4) 1828-1838 (2004)
- [4] Thompson M.W., Atchley A.A., Maccarone M.J., "Influences of a temperature gradient and fluid inertia on acoustic streaming in a standing wave", *J. Acoust. Soc. Am.*, **117** (4) 1839-1849 (2004)
- [5] Moreau S., Bailliet H., Valière J.C., "Measurements of inner and outer streaming vortices in a standing waveguide using laser doppler velocimetry", *J. Acoust. Soc. Am.*, **123** (2) 640-7 18247868 (2008)
- [6] Penelet G., Gusev V., Lotton P., Bruneau M., "Non-trivial influence of acoustic streaming on the efficiency of annular thermoacoustic prime-movers", *Phy. Let. A*, **351** Issue 4-5, 268-273 (2006)
- [7] Ceperley P.H., "A pistonless Stirling engine - the traveling wave heat engine", *J. Acoust. Soc. Am.*, **66** 1508-1513 (1979)
- [8] Ceperley P.H., "Split mode travelling wave ring-resonator", *United States Patent*, N 4, 686, 407 (1987)
- [9] Backhaus S., Swift G.W., "A thermoacoustic Stirling engine", *Nature*, **399** 335-338 (1999)
- [10] Amari M., Gusev V., Joly N., "Transient unidirectional acoustic streaming in annular resonators", *Ultrasonics*, **42** 53-56 (2004)
- [11] Lawrenson C.C., Lafleur L.D., Shields F.D., "The solution for the propagation of sound in a toroidal waveguide with driven walls (the acoustitron)", *J. Acoust. Soc. Am.*, **103**(3) 1253-1260 (1997)
- [12] Hu J., Nakamura K. Ueha S., "An analysis of a non-contact ultrasonic motor with an ultrasonically levitated rotor", *Ultrasonics*, **35** 459-467 (1997)
- [13] Biwa T., Tashiro Y., Ishigaki M., Ueda Y., Yasaki T., "Measurements of acoustic streaming in a looped-tube thermoacoustic engine with a jet pump", *J. Appl. Phys.*, **101** 064914 (2007)
- [14] Lotton P., Dalton E., Amari M., Gusev V., Joly N., "Acoustic streaming in annular resonator : application to pcr on-chip reactor", *Acte du 3ème Congrès Français de Microfluidique*, INSA, Toulouse (2006)
- [15] Job S., "Études théoriques et expérimentales d'un générateur thermoacoustique annulaire à ondes progressives", *Thèse de doctorat*, Université du Maine (2001)
- [16] Gusev V., Job S., Bailliet H., Lotton P., Bruneau M., "Acoustic streaming in annular thermoacoustic prime-movers", *J. Acoust. Soc. Am.*, **103** (3) 1253-1260 (2000)